Int. J. Electrochem. Sci., 16 **(2021)** 151019, doi: 10.20964/2021.01.47

International Journal of
ELECTROCHEMICAL
SCIENCE
www.electrochemsci.org

Microwave Synthesis of Eco-friendly Nitrogen Doped Carbon Dots for the Corrosion Inhibition of Q235 Carbon Steel in 0.1 M HCl

Mingjun Cui[1,*], *Yujie Qiang*[2], *Wei Wang*[1], *Haichao Zhao*[2], *Siming Ren*[2,*]

[1] Key Laboratory of Impact and Safety Engineering, Ministry of Education, School of Mechanical Engineering and Mechanics, Ningbo University, Ningbo, 315211, China
[2] Key Laboratory of Marine Materials and Related Technologies, Zhejiang Key Laboratory of Marine Materials and Protective Technologies, Ningbo Institute of Materials Technology and Engineering, Chinese Academy of Sciences, Ningbo, 315201, China
[*]E-mail: cuimingjun@nbu.edu.cn, rensiming@nimte.ac.cn

Received: 19 September 2020 / *Accepted:* 30 October 2020 / *Published:* 30 November 2020

In this work, nitrogen doped carbon dots (NCDs) were prepared with citric acid monohydrate ($CA{\cdot}H_2O$) and ethanolamine (EA) via microwave method. In combination with electrochemical techniques, weight loss and SEM, it is found that nitrogen doping in carbon dots effectively suppresses the corrosion of Q235 carbon steel in HCl solution owing to the presence of pyrrolic N in NCDs. Especially for NCDs (1:10), the optimum inhibition efficiency is about 89% after 1 h of immersion in 0.1 M HCl solution with 500 ppm of concentration. By further calculation, the ΔG_{ads}^{0} value for NCDs (1:10) is -26.65 $kJ{\cdot}mol^{-1}$, indicating the adsorption of NCDs on Q235 carbon steel surface involves both chemisorption and physisorption. In addition, NCDs still remain superior corrosion inhibition performance with the prolonged immersion time and ascending temperature.

Keywords: Microwave synthesis; NCDs; Corrosion inhibition; Q235 carbon steel.

1. INTRODUCTION

Acid pickling with hydrochloric acid (HCl) solution as acidic media is a common, economical and efficient industrial process to remove the undesirable incrustation and rusts of industrial equipment [1,2]. However, Q235 carbon steel, as the widely used engineering structural material in current industry, is sensitive to the corrosive environment and easily attacked by HCl solution. Hence, to alleviate the corrosion of Q235 carbon steel during the acid pickling process, the use of organic inhibitors is one of the most effective, practical and economic choices [2,3]. Commonly, organic inhibitors with heteroatoms

(O, N, S and P, etc.), aromatic rings, polar functional groups or π bonds are usually selected for this purpose, which can effectively reduce the sensitivity of metals to corrosive attack through the physical adsorption or chemical adsorption or both on the metal surface [4-7]. With the improvement in green awareness and enactment of environmental regulations, the traditional inhibitors with deleterious impacts is being precluded. Therefore, seeking eco-friendly, good water-soluble, and high-effective substitutes becomes highly urgent. For instance, Liao and coworkers found that the extract of Longan seed and peel could be used to inhibit the corrosion of mild steel in HCl solution [8]. Qiang and coworkers used the extract of ginkgo leaf as eco-friendly corrosion inhibitor to impede the corrosion of X70 steel in 1 M HCl solution [9].

Carbon dots (CDs) with high water solubility, good biocompatibility, low toxicity and unique photoluminescence (PL) properties, possess great potential application in sensors, catalysis, bioimaging and drug delivery, and have been extensively studied in recent years [10-14]. Particularly, at the year of 2017, Zhu and coworkers reported that CDs incorporated polymers showed obvious healing/self-healing behavior owing to the interfacial bonding (covalent, hydrogen, and van der Waals bonding) between the polymers and CDs with various functional groups [15]. This result indicated that it might be possible to apply CDs in the field of corrosion protection. Inspired by this report, the corrosion inhibition performance of N-doped carbon dots (NCDs) with the aminosalicylic acid and phenylenediamine as raw materials was first investigated by Cui and coworkers, and the results indicated that NCDs could effectively inhibit the corrosion of Q235 carbon steel in 1 M HCl solution [16,17]. In addition to use the aromatic compounds as precursors, Ye and coworkers reported a kind of N-doped citric acid-based carbon dots with ammonium citrate as raw materials that also exhibited high inhibition efficiency (> 90%) for the Q235 carbon steel after 24 h of immersion in 1 M HCl environment [18]. Based on this, the further investigation by Qiang and coworkers indicated that NCDs still remained superior inhibition effect for Cu substrate in 0.5 M H_2SO_4 solution at 298~318 K, although the increasing temperature could accelerate the corrosion process [19]. Owing to the high water solubility, NCDs could be homogeneously dispersed into the waterborne epoxy resin, and it was found that the corrosion protection of the composite coatings was improved significantly [20]. This is because the surface functional groups of NCDs can react with waterborne epoxy to improve the interfacial bonding between NCDs and coating matrix, thus reducing the diffusion of oxygen in the coating and delaying the corrosion of metal substrate.

From the above investigations, it could be noted that NCDs synthesized from aromatic compounds or common organic compounds with nitrogen exhibited superior corrosion inhibition performance. In some cases, NCDs can also be synthesized by two precursors, for example, citric acid as carbon source and amine organics as nitrogen source. In order to confirm whether this type of NCDs also have inhibition effect on the metal corrosion or not, a new kind of NCDs was synthesized with the citric acid monohydrate and ethanolamine as precursors in this study. Different with the above investigations, NCDs in this work were prepared via a novel microwave assisted carbonization method that strongly shortened the preparation time of NCDs. Corresponding inhibition performance for Q235 carbon steel corrosion in HCl solution was further systematically investigated in the view of concentration, immersion time and temperature by potentiodynamic polarization test, electrochemical impedance spectroscopy (EIS), weight loss and surface analysis.

2. EXPERIMENTAL SECTION

2.1. Materials

Citric acid monohydrate ($CA{\cdot}H_2O$) and ethanolamine (EA) were purchased from Shanghai Aladdin Chemical Regent Co., Ltd. (China). Ethanol, acetone and hydrochloric acid (HCl, 39%) were purchased from Sinopharm Chemical Reagent Co., Ltd (Shanghai, China). The polished Q235 carbon steel substrates with size 3×4×0.2 cm^3 and 1×1×0.1 cm^3 were purchased from local suppliers. Deionized water (DI) was used during whole experiments.

2.2. Synthesis of CDs and NCDs

EA and $CA{\cdot}H_2O$ with various molar ratio were first dissolved into 50 mL of distilled water, then the mixed solution was transferred into a domestic microwave oven (700 W), and heated for 25 min with three different heating periods.

(1) The mixed solution was heated under medium heat to remove water quickly, and regular intervals were needed to avoid bumping (5 min).

(2) The mixture was heated continuously under medium-high heat for the carbonization of reactants (10 min).

(3) The mixture was heated under high heat for 10 min to achieve a further carbonization.

The final products were collected by adding DI water to form the aqueous solution and purified with a dialysis bag (molecular weight cut-off ~ 1.0 kDa) for 1 day to remove the nonreactive molecules. The DI water would be replaced every 3 h. The purified products were collected by removing water with rotary evaporator, and dried at 80 ℃ in drying oven for 12 h, as shown in Scheme 1.

The obtained products were denoted as NCDs (1:*x*), where 1:*x* corresponds to the molar ratio of CA:EA. When the molar ratio was 1:0, the product was donated as CDs. When the molar ratio of CA:EA was 1:2, 1:6, 1:10 and 1:14, the prepared NCDs samples were marked as NCDs (1:2), NCDs (1:6), NCDs (1:10) and NCDs (1:14), respectively. Also, EA was heated under same condition for comparison and the corresponding product was named as PEA.

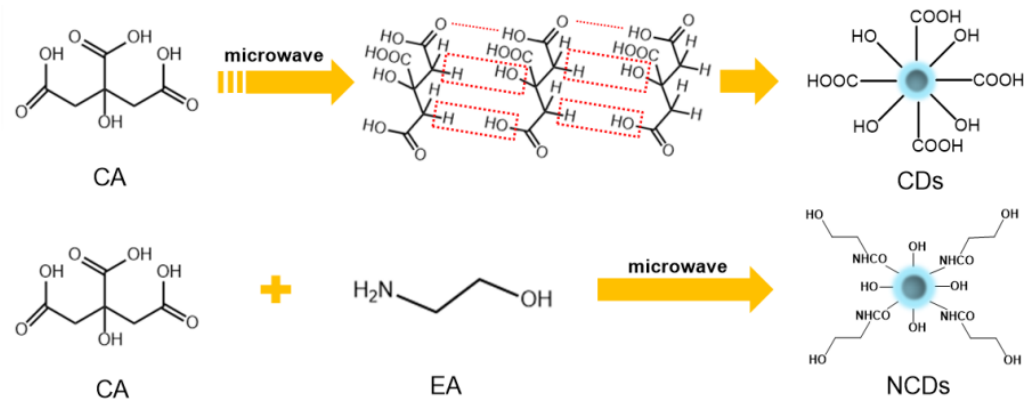

Scheme 1. Synthesis of CDs and NCDs

2.3. Preparation of electrode and electrolytic solution

Prior to the experiments, Q235 carbon steel substrates were first polished with SiC abrasive papers (300, 600 and 1200 grit), then washed with ethanol and DI water, and dried at room temperature. The corrosive medium (0.1 M HCl solution) was prepared by diluting the analytical grade 36% HCl with distilled water. 100, 300, and 500 ppm of the test solution were prepared by adding a certain quality of NCDs to 0.1 M HCl solution in the volumetric flask, and the NCDs could be dissolved completely in 0.1 M HCl solution without any precipitation. For each test, a freshly prepared electrolytic solution was used and its volume was 50 mL.

2.4. Characterization of CDs and NCDs

Micro-fourier transform infrared (Micro-FTIR, Cary660+620, America) spectra was used examine the characteristic functional groups of the inhibitors. The prepared samples could be checked directly by dipping itself on the workbench. Scanning probe microscope (SPM, Veeco Dimension 3100V, America) and transmission electron microscopy (TEM, Talos F200x, America) were performed to check the morphology and size of CDs and NCDs. For SPM and TEM studies, the samples were first dissolved in the water, and then the solution was dropped on the Si substrate and super-thin carbon-coated copper grid (200 meshes), and finally dried at 80 ℃ in drying oven. X-ray photoelectron spectroscopy (XPS, AXIS ULTRA DLD, England) was used to check the chemical composition and bonding status of samples. For NCDs samples, NCDs were directly dripped on the Si substrate ($0.5\times0.5\times0.1$ cm^3) and dried under vacuum oven for 24 h.

2.5. Electrochemical measurements

All electrochemical tests were conducted in a CHI660E electrochemical station (Chenhua, China) with a conventional three-electrode system where a platinum foil was used as counter electrode, saturated silver-silver chloride (Ag/AgCl) electrode was used as reference electrode, and the Q235 carbon steel substrate with 1 cm^2 of exposed surface area was used as the working electrode. Before the test, the working electrode was kept for an hour in the corrosive medium to record a constant open circuit potential (OCP) test. The EIS measurements were performed at OCP using 10 mV of disturbance signal from 10 kHz to 0.01 Hz. All the EIS results were analyzed with Zsimpwin software. Subsequently, the potentiodynamic polarization plots were recorded in the potential range of ± 250 mV with respect to the OCP at a scan rate of 1 $mV \cdot s^{-1}$. The corrosion current density (i_{corr}) and corrosion potential (E_{corr}) values could be obtained from polarization curves by Tafel extrapolation method. And corresponding inhibition efficiency (η) is calculated according following equation [16,17,21]:

$$\eta = \frac{i_{corr}^0 - i_{corr}}{i_{corr}^0} \times 100 \qquad (1)$$

where $i_{corr}^0$and i_{corr} is the corrosion current density in the absence and presence of inhibitors, respectively.

2.6. Weight loss measurement

The weight loss measurement was carried out according to ASTM standard G1-03. Q235 carbon steel substrates with a dimension of 1×1×0.1 cm^3 were immersed in 0.1 M HCl solution in the absence and presence of synthetic inhibitors (CDs, PEA and NCDs with various molar ratio of CA:EA and concentrations) at 298 K. Then the specimens were taken out at various immersion times, washed with DI, dried and weighed accurately. To ensure the reliability of the results, at least three parallel specimens were tested. The weight loss was defined as the mass difference of the specimen before and after immersion in corrosive medium, and their average values were used for the calculations.

The corrosion rate (*CR*) and surface coverage (θ) of various specimens at different immersion times are calculated according to the weight loss measurement, as shown in the following equations [5,19,22,23]:

$$CR = \frac{\Delta M}{At} = \frac{M_1 - M_2}{At} \quad (2)$$

$$\theta = \frac{CR_{HCl} - CR_{inhibitor}}{CR_{HCl}} \quad (3)$$

where *CR* ($mg \cdot cm^{-2} \cdot h^{-1}$) is the corrosion rate of the Q235 carbon steel substrates in various corrosive medium. M_1 and M_2 is the weight of specimens before and after immersion in corrosive medium, respectively. ΔM is the average weight loss (mg), *A* is the surface area of the specimen (cm^2), and *t* is the immersion time (h). CR_{HCl} and $CR_{inhibitor}$ is the corrosion rate in the absence and presence of inhibitors, respectively.

2.7. Surface Analysis

The surface information of Q235 carbon steel before and after immersion in various corrosive medium was analyzed by scanning electron microscope (SEM, Zeiss) and X-ray photoelectron spectroscopy (XPS, AXIS ULTRA DLD, England) was used to check the chemical composition and bonding status of samples. The Q235 carbon steel sheets (1×1×0.1 cm^3) after immersion in corrosive medium were used for a surface analysis.

3. RESULTS AND DISCUSSION

3.1. Characterization of CDs and NCDs

TEM and SPM were used to characterize the morphology of CDs and NCDs. It can be noted from the TEM and SPM results that most of CDs and NCDs are mono-dispersed uniformly while there are still some aggregated CDs and NCDs. HRTEM images of the selected particles reveal a lattice spacing distance of 2.05 Å and 2.08 Å for CDs and NCDs (upper insets of Figure 1a and b), corresponding to the in-plane lattice spacing of graphite ((100) facet) [24,25]. Besides, the SPM results in Figure 1c-d show that CDs and NCDs have pseudo-spherical structure with different particle size. The particle size of CDs is uneven, and the topographic height (vertical distance) ranges from 6.0 nm to 15.0

nm. In case of the NCDs, the particle size is relative small and the topographic height varied between 4.0 nm and 7.0 nm.

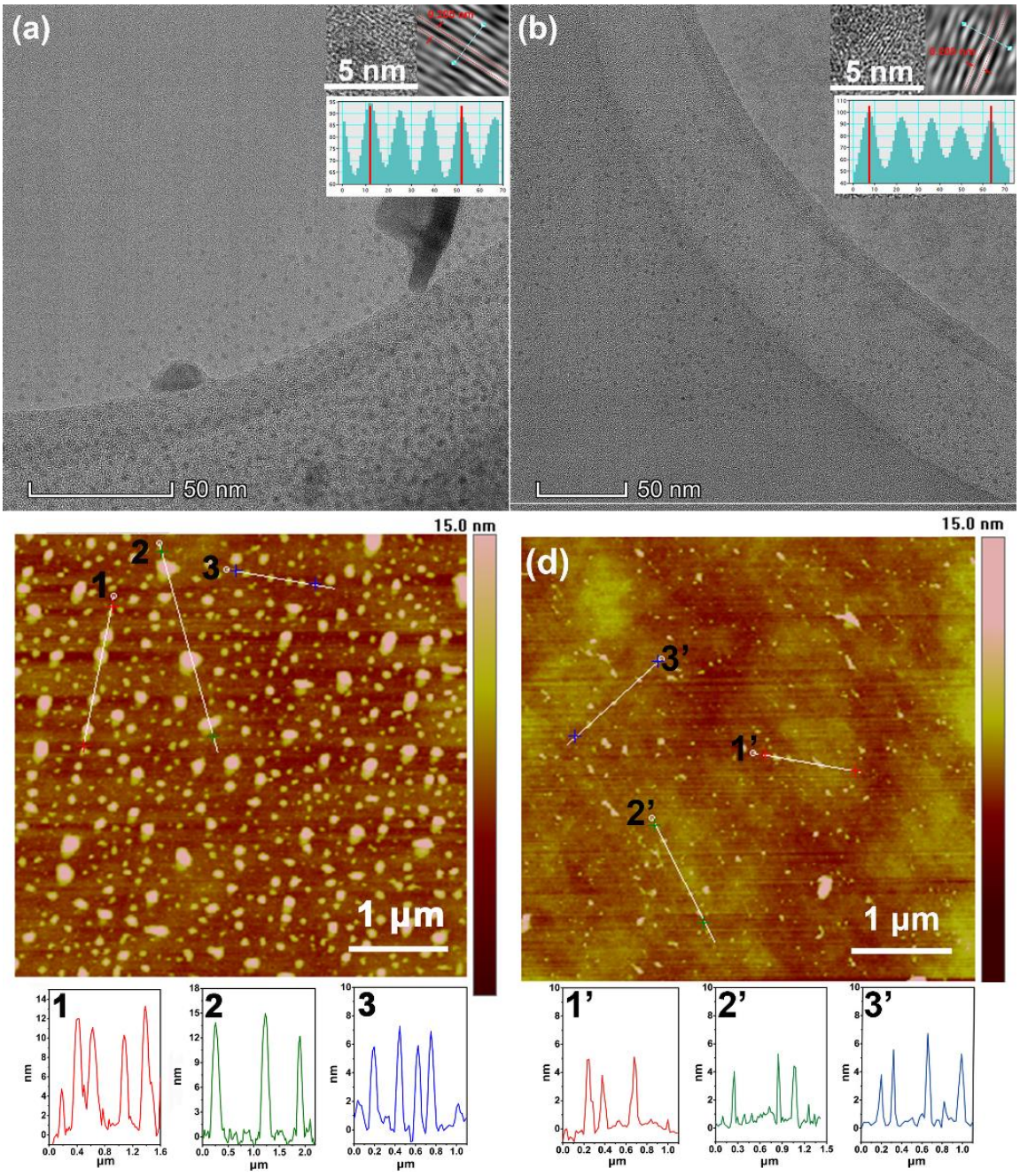

Figure 1. TEM (insert HRTEM) and SPM images with height profiles for CDs (a and c) and NCDs (b and d)

The comparison of FTIR spectra among CA, CDs, EA, PEA and NCDs with various molar ratios is shown in Figure 2a. All samples exhibit two broad peaks at 3200~3550 cm^{-1} assigned to O−H stretching vibration of carboxylic acid and $–NH_2$ stretching vibration, and at 2800~3020 cm^{-1}

corresponding to C−H vibration [11,24,26]. After the microwave process, CA is carbonized, and the prepared CDs display strong C=O stretching vibration (carbonyl) at 1705 cm^{-1}, confirming the presence of carboxylic functional group on the surface of CDs. In case of EA, there is little variation for the FTIR of EA and PEA after the microwave process. However, when CA is added, the FTIR spectra of prepared NCDs are quite different from those of CA, EA, PEA and CDs. It is observed that NCDs display strong absorption peaks at 1550 and 1400 cm^{-1} corresponding to the N−H bending variation and amide C−N stretching variation, respectively, indicating that EA has reacted with carboxylic groups on the CDs forming the amide group [10,27,28].

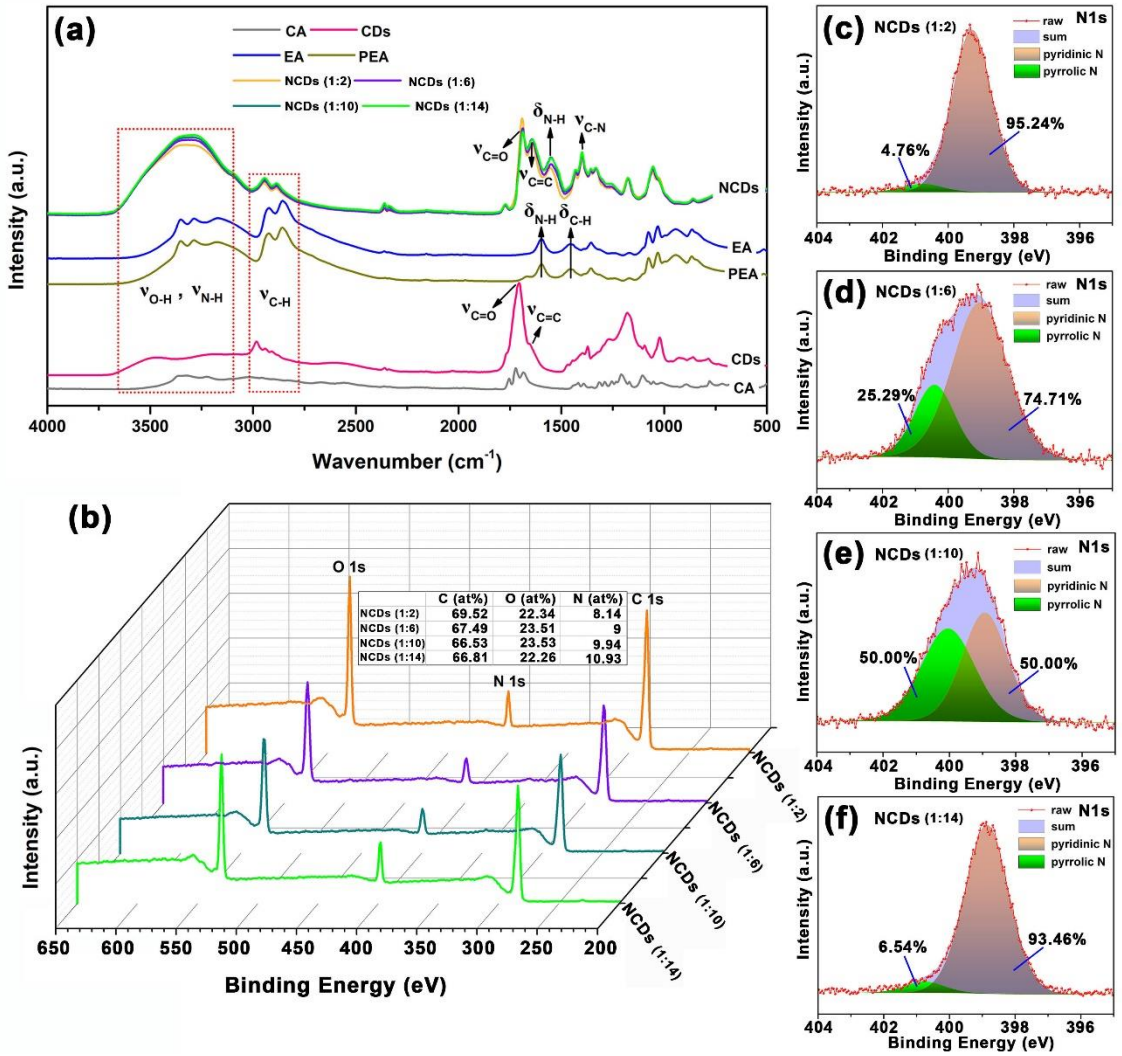

	C (at%)	O (at%)	N (at%)
NCDs (1:2)	69.52	22.34	8.14
NCDs (1:6)	67.49	23.51	9
NCDs (1:10)	66.53	23.53	9.94
NCDs (1:14)	66.81	22.26	10.93

Figure 2. (a) FTIR spectra of CA, CDs, EA, PEA and NCDs with various molar ratios, (b) XPS survey scans and corresponding atomic contents of C, N and O atoms, as well as N1s spectra for NCDs with various molar ratio of CA:EA ((c) 1:2, (d) 1:6, (e) 1:10, (f) 1:14)

Subsequently, the variations of chemical compositions and bonds for different NCDs are checked via XPS spectra. It can be noted from Figure 2b that NCDs consist of C, N and O, and the concentration of nitrogen increases from 8.14 at% to 10.93 at% with the molar ratio of NCDs varying from 1:2 to 1:14.

Detailed analysis on N1s spectra for all NCDs is shown in Figure 2c-f, in which two component peaks are ascribed to the pyridinic N and pyrrolic N [17,29]. However, owing to the different reaction degrees between CA and EA, the area ratio of pyridinic N and pyrrolic N for different NCDs is different, where the area ratio of pyrrolic N increases first and then decreases with the molar ratio of NCDs varying from 1:2 to 1:14.

3.2. Effects of molar ratio (CA:EA) and concentration

3.2.1 Potentiodynamic polarization measurements

The inhibition effect of NCDs with various molar ratios and concentrations on the corrosion of Q235 carbon steel substrates in 0.1 M HCl solution at 298 K was investigated by potentiodynamic polarization, and corresponding results were shown in Figure 3. With respect to the blank HCl solution, a significant decrease in anodic current density and a shift toward more positive corrosion potential for the polarization plots can be observed after the addition of CDs, PEA and NCDs in 0.1 M HCl solution, indicating the addition of the inhibitors weakens the anodic dissolution of Q235 carbon steel.

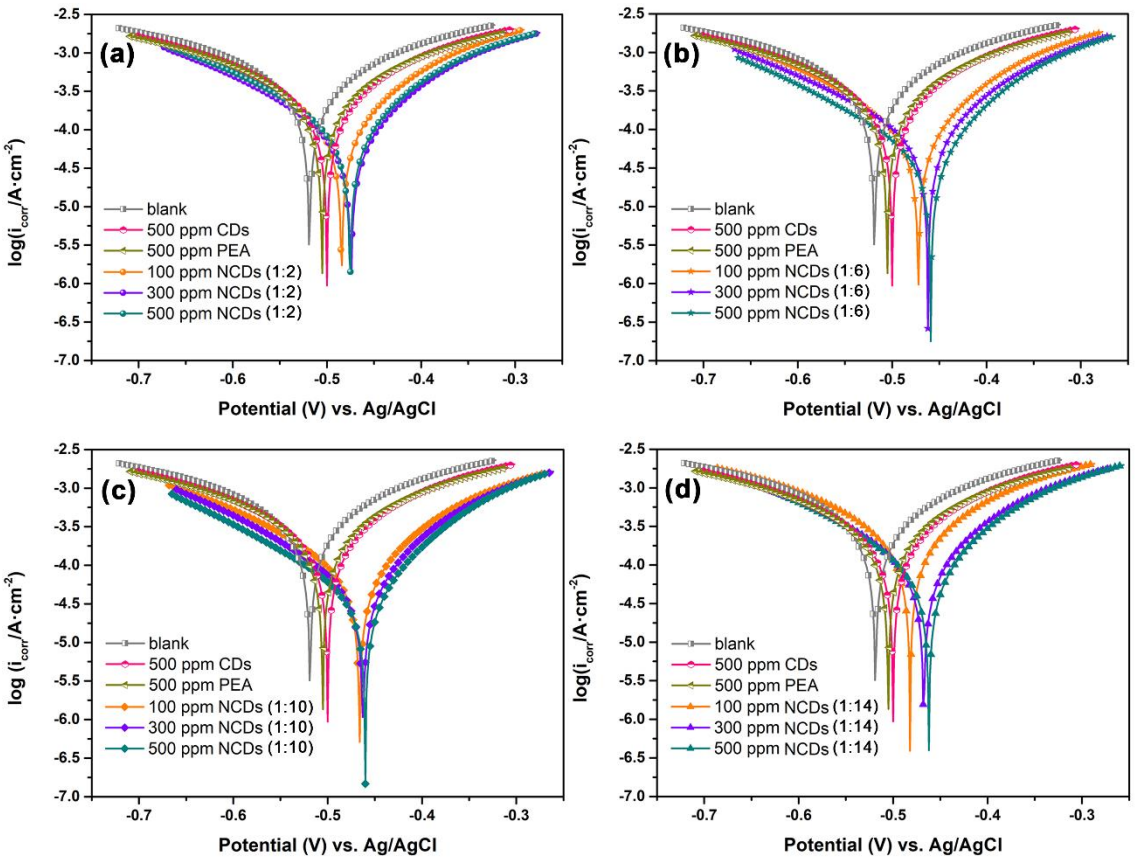

Figure 3. The potentiodynamic polarization plots for Q235 carbon steel substrates in 0.1 M HCl solution in the absence and presence of various concentrations of NCDs at 298 K, (the molar ratio of CA:EA for the prepared NCDs is (a) 1:2, (b) 1:6, (c) 1:10, (d) 1:14, respectively)

Further, the values of corrosion current density (i_{corr}) and corrosion potential (E_{corr}) obtained from the polarization plots, as well as the inhibition efficiency (η) calculated according to Eq. (1) are summarized in Table 1. An inspection of the data in Table 1 reveals that, at room temperature, the addition of NCDs in 0.1 M HCl solution results in lower i_{corr}, more positive E_{corr} and higher η values as compared with CDs and PEA, which indicates that the incorporation of nitrogen can improve the inhibition efficiency of CDs. For the NCDs with a constant molar ratio (except for NCDs (1:2)), i_{corr} values decrease gradually with the increasing NCDs concentration. The corresponding E_{corr} and η also increase with the NCDs concentration. For the NCDs at a constant concentration, the samples exhibit lower i_{corr}, more positive E_{corr} and higher η values for the NCDs (1:10) than others, and the order of η is as follows: 1:2 < 1:6 < 1:10 > 1:14. It is noteworthy that this order is consistent with the variation on the area ratio of pyrrolic N in NCDs, indicating that the content of pyrrolic N in NCDs has closely relation with the corrosion inhibition efficiency of NCDs. By further comprehensive analysis, it can be concluded that NCDs (1:10) shows the superior corrosion inhibition (i_{corr}: 45.7 μA·cm^{-2}, E_{corr}: -0.46 V, η: 89.04%) for Q235 carbon steel in 0.1 M HCl solution. The largest displacement in E_{corr} value observed at a concentration of 500 ppm for 1:10 NCDs is 59 mV, which is much less than 85 mV, suggesting NCDs is a mixed-type inhibitor [30,31]. These results indicate that NCDs with high concentration of pyrrolic N are prone to effectively inhibit the corrosion of metals in 0.1 M HCl solution.

Table 1. The variation of corrosion current density (i_{corr}), corrosion potential (E_{corr}) and inhibition efficiency values (η) for the Q235 carbon steel substrates in 0.1 M HCl solution in the absence and presence of CDs, PEA and NCDs with various molar ratio of CA:EA and concentrations

Samples	Concentration (ppm)	i_{corr} (μA· cm^{-2})	E_{corr} (mV)	Inhibition efficiency (η)
blank	/	417	-519	/
CDs	500	252	-500	39.51
PEA	500	290	-505	30.45
NCDs (1:2)	100	140	-484	66.51
	300	88.7	-474	78.76
	500	109	-475	73.83
NCDs (1:6)	100	104	-472	75.11
	300	94.0	-462	77.45
	500	57.3	-459	86.27
NCDs (1:10)	100	90.9	-466	78.23
	300	60.2	-463	85.58
	500	45.7	-460	89.04
NCDs (1:14)	100	233	-482	44.18
	300	115	-468	72.54
	500	94.4	-462	77.39

3.2.2 Electrochemical impedance spectroscopy measurements

Electrochemical impedance spectroscopy (EIS) measurements are further performed to investigate the corrosion behavior of Q235 carbon steel substrates in 0.1 M HCl solution in the absence and presence of inhibitors. Figure 4 displays the Nyquist plots and Bode plots for Q235 carbon steel

substrates in 0.1 M HCl solution without and with 500 ppm of CDs and PEA. The Nyquist plots (Figure 4a) show a depressed capacitive loop assigned to the charge transfer process at electrode/solution interface at the high frequency both in the blank and in the presence of CDs and PEA, and the diameter of capacitive loop increases remarkably after the addition of CDs and PEA. The deviation from an ideal to depressed semicircle is due to the inhomogeneity and roughness of the steel surface [21,31,32]. Besides, a small inductive loop appears at low frequencies owing to the relaxation process like Cl^-_{ads} and H^+_{ads} on the metal substrates [17,33]. Similarly, it is distinct from the Bode plots (Figure 4b) that the addition of CDs and PEA results in the increase in the impedance modulus, and the sample immersed in 0.1 M HCl solution with 500 ppm of CDs exhibits the highest impedance modulus (150 Ω cm^2). The single peak in the Bode-phase angle plots (Figure 4b) further suggests a single time constant for the corrosion process at the metal-solution interface for all samples. And the peak height with the addition of inhibitor is higher than that of blank, indicating a more capacitive response owing to the presence of inhibitor molecules at the interface.

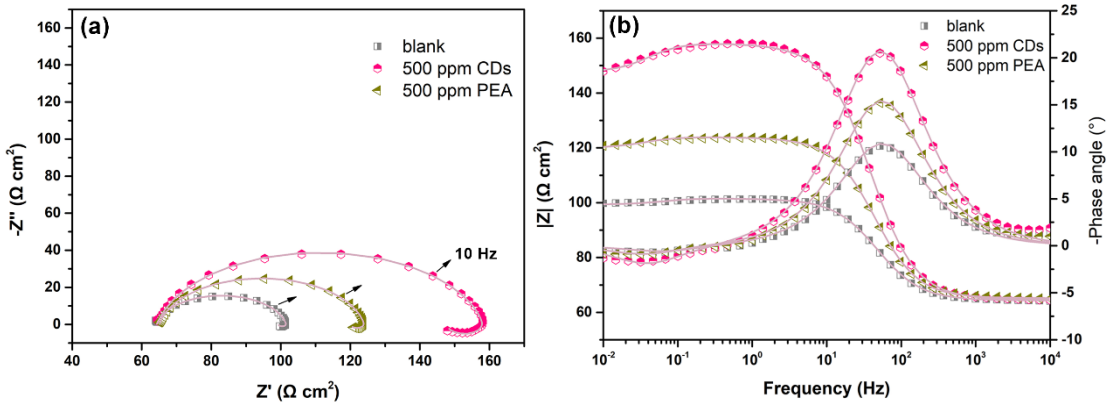

Figure 4. The Nyquist (a) and Bode (b) plots of Q235 carbon steel in 0.1 M HCl solution in the absence and presence of CDs and PEA at room temperature

The corrosive behavior of Q235 carbon steel in 0.1 M HCl solution in the presence of NCDs with various molar ratios and concentrations was also investigated. As shown in Figure 5, the shape of EIS plots for all samples is similar with the EIS results in Figure 4, indicating that the electrochemical characteristics of the solution haven't been varied with the addition of NCDs due to the relatively looser adsorption films [4]. The capacitive loop at high frequency (HF) and inductive loop at low frequency (LF) can also be observed for the Nyquist plots of all samples (Figure 5c, e and g), and the continuous expansion for the diameters of Nyquist plots indicates an ascending trend of inhibition efficiency with the increasing concentration, irrespective of the molar ratio of NCDs (except for NCDs (1:2)). The impedance modulus and peak height in Bode plots (Figure 6d, f and h) also display a similar variation tendency.

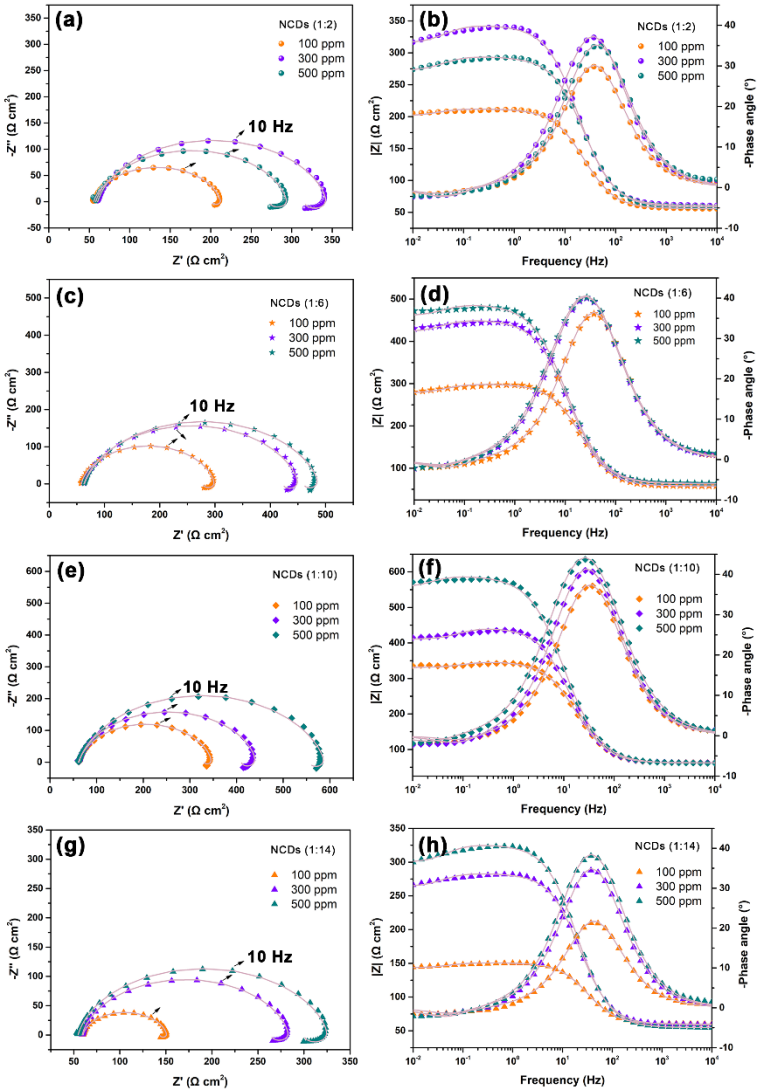

Figure 5. The Nyquist and Bode plots of Q235 carbon steel in 0.1 M HCl solution in the presence of NCDs with various concentrations at room temperature, (The molar ratio of CA:EA for prepared NCDs is (a, b) 1:2, (c, d) 1:6, (e, f) 1:10, (g, h) 1:14)

Therefore, it can be concluded based on the EIS results that the optimal concentration for the NCDs with a molar ratio of 1:6, 1:10 and 1:14 is 500 ppm. In case of (1:2) NCDs, the diameter of Nyquist plots (Figure 5a), impedance modulus and peak height in Bode plots (Figure 5b) increase first and then decrease with the increasing concentration, and the optimal concentration is 300 ppm. Compared to the samples in the presence of CDs and PEA, the samples immersed in 0.1 M HCl solution with NCDs show higher impedance, indicating high inhibition efficiency of these NCDs. Furthermore, the molar ratio of CA:EA plays an important role on the inhibition ability of NCDs. It is apparent that the samples immersed in 0.1 M HCl solution with NCDs (1:10) show the highest impedance modulus (~560 Ω cm^2), indicating 500 ppm of NCDs (1:10) has excellent inhibition ability against the corrosion of Q235 carbon steel.

Ulteriorly, the EIS data in Figure 4 and Figure 5 are analyzed in terms of equivalent electrical circuit (EEC) in Figure 6, where R_s, R_{ct}, CPE_{dl}, L and R_L represent the solution resistance, the charge transfer resistance, the double layer capacitance, the inductance and inductive resistance, respectively.

The use of CPE_{dl} instead of an ideal capacitor is attributed to the different physical phenomena like surface roughness, inhibitor adsorption and porous layer formation [17,31,34-36]. The inductance L in the EIS results is closely related with the relaxation process occurred by adsorption species (such as Cl^-_{ads} and H^+_{ads}) on the surface metal. Even in the presence of the inhibitor, the inductance still appears, implying that the dissolution of Q235 carbon steel is still going on through the direct charge transfer. The data obtained from the EEC such as R_s, R_{ct}, CPE_{dl}, n, L and R_L are summarized in Table 2. It is clear from Table 2 that the R_{ct} value increases greatly after the addition of various inhibitors (especially for NCDs) in 0.1 M HCl solution, which is caused by the formation of absorption film at the metal/solution interface. To the contrary, the decrease in CPE_{dl} values is also observed owing to the decrease in the local dielectric constant or an increase in the thickness of the electrical double layer or both, also proving the absorption of inhibitor molecules at the metal/solution interface [37]. Furthermore, the variation on the R_{ct} value obtained from the fitting of EEC is in good agreement with the EIS results, and the largest inhibition effect is observed at 500 ppm of NCDs (1:10), which gives a R_{ct} value equal to 529.7 Ω cm^2.

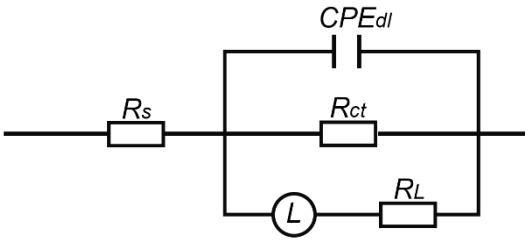

Figure 6. The equivalent electrical circuit (EEC) to fit the EIS results in Figure 4 and 5

Table 2. The fitting electrochemical parameters obtained from EIS results for the Q235 carbon steel sample immersed in 0.1 M HCl solution in the absence and presence of various NCDs with various molar ratio of CA:EA and concentrations at room temperature

	R_s (Ω cm^2)	CPE_{dl} (F cm^{-2})	n	R_{ct} (Ω cm^2)	L (H)	R_L (Ω cm^2)
blank	64.19	1.91e-4	0.8813	37.48	1480	574.7
500 ppm CDs	64.44	1.00e-4	0.8813	93.87	3240	747.2
500 ppm PEA	65.02	1.24e-4	0.8966	58.86	3939	820.7
			NCDs (1:2)			
100 ppm	55.55	9.76e-5	0.8859	157.1	1.08e4	2040
300 ppm	60.41	7.23e-5	0.8782	283.9	1.02e4	2547
500 ppm	58.04	6.89e-5	0.8793	236.8	9957	2265
			NCDs (1:6)			
100 ppm	57.93	7.20e-5	0.8949	241.7	9918	2492
300 ppm	62.75	8.58e-5	0.8631	390.2	2.17e4	4751
500 ppm	63.52	8.9e-5	0.8492	426.6	2.51e4	5869
			NCDs (1:10)			
100 ppm	62.3	7.21e-5	0.8873	286.2	7510	4480
300 ppm	62.01	7.12e-5	0.881	382.6	8080	3969

500 ppm	61.11	7.53e-5	0.8523	529.7	5.36e4	7756
			NCDs (1:14)			
100 ppm	60.06	1.14e-4	0.8972	91.09	3156	996.2
300 ppm	59.15	7.20e-5	0.8926	224.7	1.02e4	2313
500 ppm	54.66	7.08e-5	0.8844	272.1	9164	2496

3.2.3 Weight loss analysis

The influence of immersion time on the corrosion of Q235 carbon steel in 0.1 M HCl solution in the absence and presence of inhibitors was investigated by weight loss measurement. Figure 7 shows the evolution of corrosion rate as a function of immersion time. It is clear that the corrosion rate for all samples decreases with increasing immersion time, which may be caused by the decrease of H^+ concentration or the adsorption of inhibitors or both. In addition, there is slightly different between the electrochemical results and weight loss analysis. The corrosion rates for the samples immersed in 0.1 M HCl solution with CDs, PEA and NCDs (1:2) are equal or greater than that in blank solution during the whole immersion process, indicating the these inhibitors have almost no inhibition effect on the corrosion of Q235 carbon steel. For NCDs with a molar ratio of 1:6, 1:10 and 1:14, the corrosion rates of samples decrease remarkably with respect to that in blank solution, and decline gradually with increasing concentrations. The minimum corrosion rate (~0.034 $mg \cdot cm^{-2} \cdot h^{-1}$) is obtained from the sample after 72 h of immersion in 0.1 M HCl solution with 500 ppm of NCDs (1:10), which is consistent with the EIS results in Figure 5.

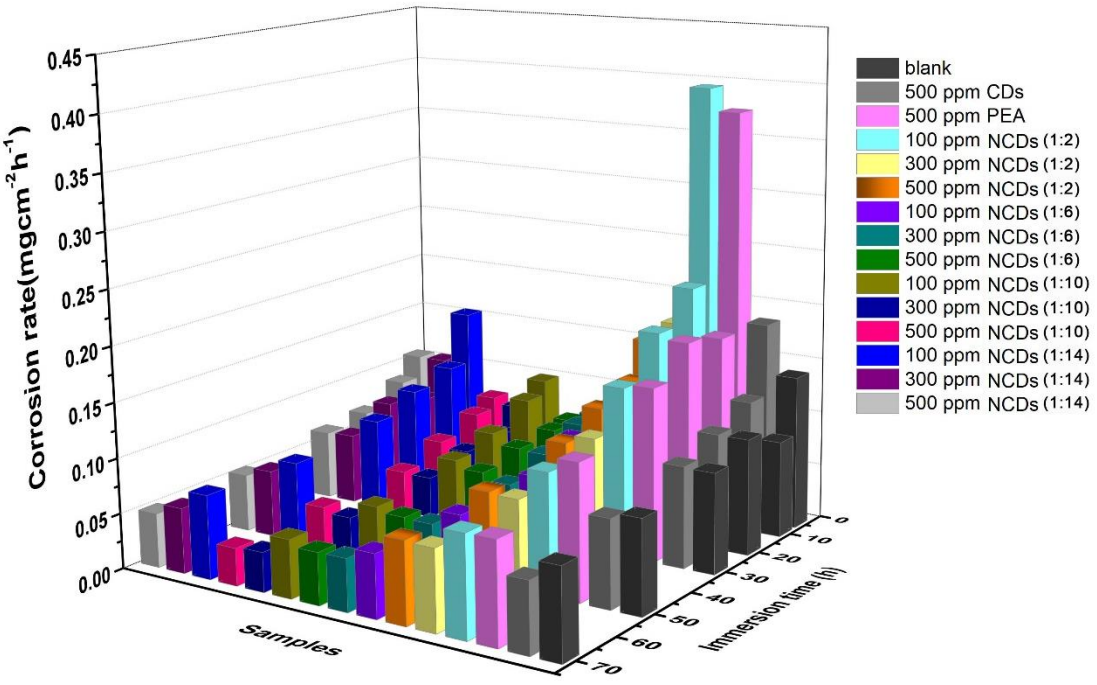

Figure 7. Variation of corrosion rate for the Q235 carbon steel substrates immersed in 0.1 M HCl solution in the absence and presence of various NCDs (the molar ratio of CA:EA for prepared NCDs is 1:2, 1:6, 1:10 and 1:14, respectively)

3.3. Adsorption Isotherm and Surface analysis

In general, the appearance of inhibition effect is attributed to a process that the adsorbed water molecules on metal surface are substituted by inhibitor molecules [23]. The inhibition efficiency of inhibitors closely depends on their adsorption behavior on the metal surface. In order to understand the possible adsorption behavior occurring on the metal surface, the classical Langmuir adsorption model (Eq. 4) is applied to fit the surface coverage (θ) of inhibitor with various concentrations [35,38].

$$\frac{C_{inh}}{\theta} = \frac{1}{K_{ads}} + C_{inh} \qquad (4)$$

where C_{inh} is the inhibitor concentration, θ is the surface coverage that is calculated according to the Eq. 3, and K_{ads} is the adsorption equilibrium constant.

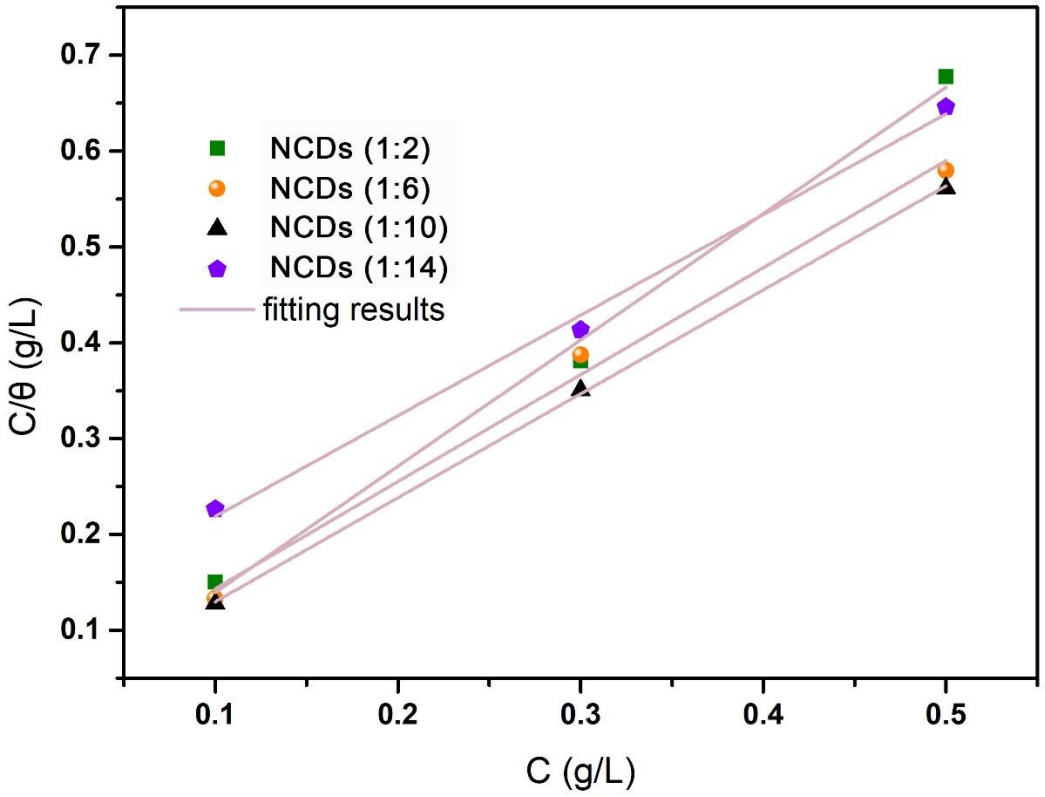

Figure 8. Adsorption isotherm deriving from the gravimetric analysis of Q235 carbon steel immersed in 0.1 M HCl solution in the presence of NCDs with various molar ratio of CA:EA according to the Langmuir model

Figure 8 shows the plots of C_{inh}/θ versus C_{inh} obtained from the gravimetric analysis and corresponding fitting results are summarized in Table 3. It is clear from Figure 8 that there is a good linear correlation between C_{inh}/θ and C_{inh} for NCDs with four different molar ratios (the regression coefficient varies from 0.9872 to 0.9995), indicating that the adsorption behavior obeys the Langmuir adsorption isotherm. The K_{ads} value is 130.38, 31.39, 46.84 and 8.78 for NCDs with molar ratio of 1:2, 1:6, 1:10 and 1:14, respectively. Besides, K_{ads} is closely related to the standard free energy of adsorption

(ΔG_{ads}^0) that can be used to evaluate the interaction between inhibitor molecules and the metal surface according to the following equation [18,39,40,41]:

$$\Delta G_{ads}^0 = -RTln(1000K_{ads}) \quad (5)$$

where R is the molar gas constant (8.314 J·mol^{-1}·K^{-1}) and T stands for the thermodynamic temperature (298 K). In addition, to keep the units same in the above equation, 1000 g·L^{-1} is used instead of 55.5 mol·L^{-1} for the mass concentration of water [17,19,30]. The ΔG_{ads}^0 value of NCDs with four different molar ratios is -29.18, -25.65, -26.65 and -22.50 kJ·mol^{-1}, respectively. The calculated ΔG_{ads}^0 value varies between -20 and -40 kJ·mol^{-1}, indicating the adsorption behavior of inhibitor molecules on metal surface is a mixed interaction of physisorption and chemisorption. Furthermore, the ΔG_{ads}^0 value for all cases is closer to -20 kJ·mol^{-1}, suggesting that physisorption is more dominant for the inhibitor molecules on steel surface. Usually, the higher $|\Delta G_{ads}^0|$ value is, the stronger adsorption capability is. Therefore, combined with electrochemical, gravimetric and surface analysis, NCDs (1:10) have better inhibition effect on the corrosion of Q235 carbon steel than others.

Table 3. Thermodynamic parameters of adsorption for Q235 carbon steel in 0.1 M HCl solution in the presence of NCDs with various molar ratio of CA:EA from Langmuir adsorption isotherm

Molar ratio	y	R^2	K_{ads}	ΔG_{ads}^0 (kJ·mol^{-1})
NCDs (1:2)	1.3172x+0.00767	0.9897	130.38	-29.18
NCDs (1:6)	1.1161x+0.03186	0.9872	31.39	-25.65
NCDs (1:10)	1.084x+0.02135	0.9995	46.84	-26.65
NCDs (1:14)	1.049x+0.1139	0.9923	8.78	-22.50

Further, the surface information of Q235 carbon steel before and after 72 h of immersion in both blank and inhibited solutions was checked by SEM. It is observed from Figure 9a that the polished Q235 carbon steel is relative smooth with some polished scratches. In case of Q235 carbon steel immersed in 0.1 M HCl solution (Figure 9b), the surface is highly corroded, and becomes very rough and porous. After the addition of 500 ppm CDs (Figure 9c) and PEA (Figure 9d), the corrosion degree become slighter than that in blank, while some cracks, pits and flakes are still observed at the Q235 carbon steel surface, indicating that the inhibition effect of CDs and PEA is not obvious. When the 500 ppm of NCDs (1:10) are added in 0.1 M HCl solution, the corrosion of Q235 carbon steel surface seems light and the polished scratches are still very clear (Figure 9e). These results indicate that the addition of NCDs effectively inhibit the corrosion of Q235 carbon steel.

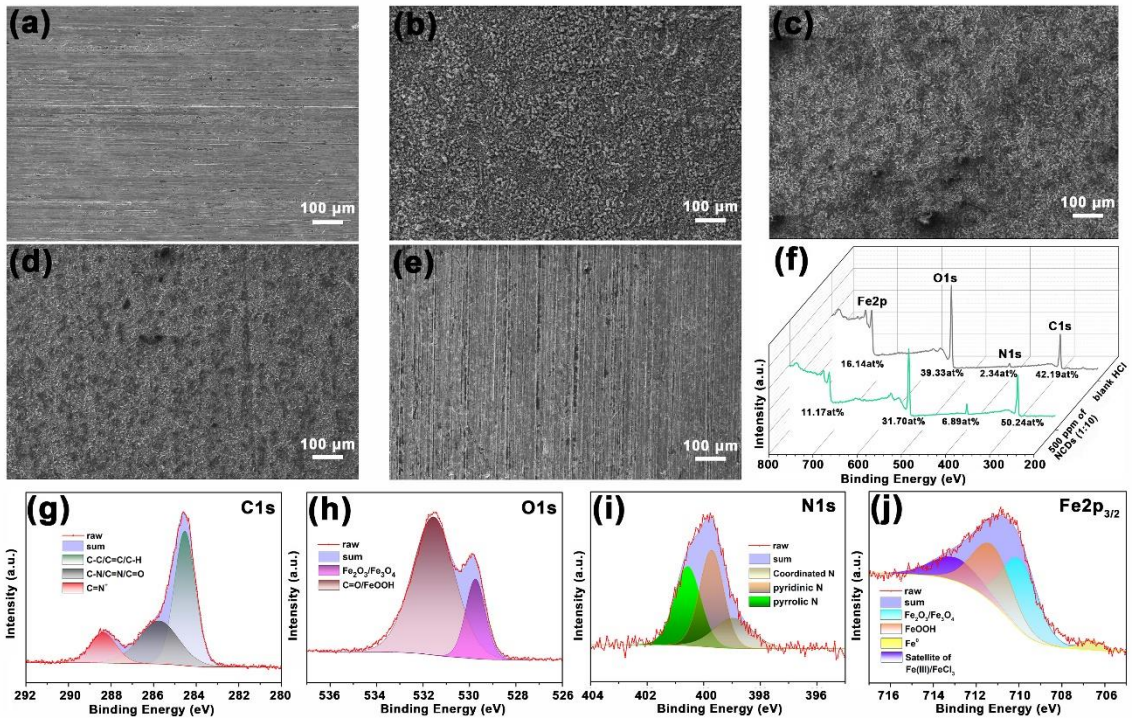

Figure 9. SEM micrographs of Q235 carbon steel surface before and after 72 h of immersion, (a) polished Q235 carbon steel, (b) in 0.1 M HCl, and in presence of 500 ppm of (c) CDs, (d) PEA and (e) NCDs (1:10), (f) XPS spectra of Q235 carbon steel in the absence and presence of NCDs, and high-resolution X-ray photoelectron deconvoluted profiles of (g) C1s, (h) O1s, (i) N1s and (j) Fe $2p_{3/2}$ for NCDs treated Q235 carbon steel.

To evidently confirm the absorption of NCDs on Q235 carbon steel, XPS analysis was used to check the variation on element content of Q235 carbons steel after 72 h of immersion in 0.1 M HCl solution in the absence and presence of 500 ppm of NCDs (1:10). Theoretically, nitrogen is absent for Q235 carbon steel immersed in 0.1 M HCl solution. However, as shown in Figure 9f, the atomic concentration of N for Q235 carbon steel is about 2.34 at% after 72 h of immersion in 0.1 M HCl solution owing to the contamination of sample by air. In case of the sample immersed in 0.1 M HCl solution with 500 ppm of NCDs (1:10), the atomic concentration of N increases remarkably to 6.89 at%, indicating the absorption of NCDs on the sample surface. Subsequently, the XPS spectra for Q235 carbon steel treated with NCDs (C1s, O1s, N1s and Fe2p) were fitted using the Casa XPS software, as shown in Figure 9g-j. And the XPS spectra were corrected by using the C 1s peak of adventitious carbon at a binding energy of 284.6 eV [42]. The C 1s spectrum are fitted into three peaks located at 284.7, 285.7 and 288.4 eV, respectively (Figure 9g). The peak at 284.7 eV was attributed to the presence of contaminant hydrocarbons and the C-C, C=C and C-H bonds of NCDs [32]. The second peak at 285.7 eV is associated with the presence of C-N, C=N and C=O groups in NCDs [32,43]. The last peak at 288.4 eV may be due to the N-C=O in NCDs or the C^+-O that may be derived from the protonation of the carbonyl groups of NCDs in HCl solution [32,44]. The O1s spectrum can be fitted with two peaks that are assigned to Fe_2O_3/Fe_3O_4 (530.0 eV) and FeOOH/C=O (531.6 eV), respectively (Figure 9h), which is consistent with the presence of the iron oxide/hydroxide in Fe $2p_{3/2}$ spectrum (Figure 9j). The

N 1s spectrum confirms that NCDs are chemically adsorbed on Q235 carbon steel surface. It can be noted from Figure 9i that N1s spectrum may be fitted into three peaks, in which two intense peaks located at 399.7 and 400.6 eV correspond to the pyridinic N and pyrrolic N, respectively, and the less intense peak at 398.9 eV may be attributed to the coordination of pyrrolic N with Fe atom of steel surface. This result suggests that NCDs-Fe complex is formed based on the donor acceptor interactions between N atoms of NCDs and the vacant d orbitals of Fe, evidencing the adsorption of NCDs on Q235 carbon steel surface [32,43].

3.4. Effect of temperature

The effect of temperature on the corrosion behavior of Q235 carbon steel in 0.1 M HCl solution with 500 ppm of NCDs (1:10) is further studied under various temperature conditions by electrochemical techniques. The typical Nyquist plots for Q235 carbon steel after 1 h of immersion in 0.1 M HCl solution in the absence and presence of 500 ppm of NCDs (1:10) at various temperatures are shown in Figure 10. The EIS results are further fitted with EECs and corresponding fitting results are summarized in Table 4. Regardless of the absence and presence of NCDs, the Nyquist plots display a semicircle and an inductive loop, except for the Nyquist plot in 0.1 M HCl at 353K. At the first case, the EEC in Figure 6 can be used to fit the EIS results. For the Nyquist plot in 0.1 M HCl at 353K, the high temperature makes the relaxation process occurred by adsorption species (such as Cl_{ads}^{-} and H_{ads}^{+}) disappear from the surface metal. Hence, the EEC should be composed of solution resistance (R_s), charge-transfer resistance (R_{ct}), and constant-phase angle element of double layer (CPE_{dl}), as shown in Figure 10a. Moreover, the diameter of semicircle decreases remarkably with the increasing temperature, indicating that the corrosion process is still controlled by the charge transfer process and the corrosion process of the steel is accelerated under higher temperature. As shown in Table 4, the R_{ct} value in the case of 500 ppm of NCDs (1:10) is higher than that in blank solution at all times, which proves that NCDs (1:10) have excellent inhibition effect even under the high temperature. Furthermore, similar conclusions can also be obtained from the polarization plots. Figure 10c and d show that the plots shift towards higher current density and positive corrosion potential with the ascending temperature (from 298 K to 353 K) for the samples immersed in these two solutions, which may be caused by the accelerated corrosion reactions or the decrease in adsorption of inhibitor molecules on metal surface or the desorption process of NCDs [22]. Besides, as shown in Table 5, i_{corr} value increases remarkably and E_{corr} mainly shows a positive shift as the temperature rises from 298 K to 353 K regardless of the absence or presence of NCDs.

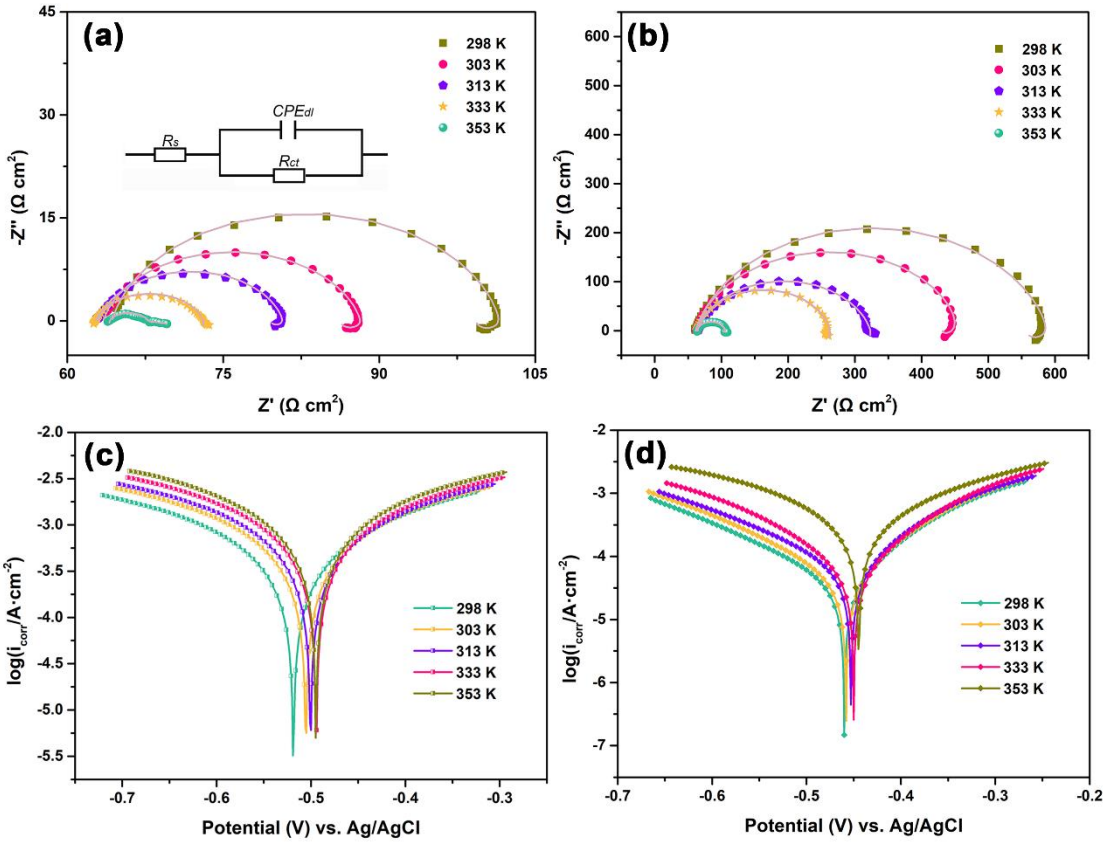

Figure 10. Nyquist and potentiodynamic polarization plots for Q235 carbon steel in 0.1 M HCl solution in the absence (a, c) and presence of (b, d) 500 ppm of NCDs (1:10) under various temperatures

Table 4. The fitting electrochemical parameters obtained from EIS results for the Q235 carbon steel sample immersed in 0.1 M HCl solution in the absence and presence of 500 ppm of NCDs (1:10) at different temperature

Samples	*T (K)*	*R_s (Ω cm^2)*	*CPE_{dl} (F cm^{-2})*	*n*	*R_{ct} (Ω cm^2)*	*L (H)*	*R_L (Ω cm^2)*
blank	298	64.19	1.91e-4	0.8813	37.48	1480	574.7
	303	63.50	2.57e-4	0.8677	24.78	1507	286.3
	313	62.97	3.10e-4	0.8662	17.81	306.1	246.8
	333	62.52	7.84e-4	0.8306	10.39	568.4	100
	353	63.89	1.17e-2	0.4774	5.16	/	/
500 ppm NCDs (1:10)	298	61.11	7.53e-5	0.8523	529.7	5.36e4	7756
	303	61.54	7.64e-5	0.863	400.2	4137	4974
	313	64.33	9.6e-5	0.8444	259.4	1.13e5	1601
	333	63.02	8.44e-5	0.884	200.5	1690	2505
	353	63.68	1.31e-4	0.8819	43.03	399	375.4

Nevertheless, i_{corr} and E_{corr} values for the samples in 0.1 M HCl with 500 ppm NCDs (1:10) are always lower (close to an order of magnitude) or more positive (close to 50 mV) than those in blank solution at each temperature (Table 5). More importantly, the η value varies slightly with the increase in

temperature from 298 K to 333 K. Until the temperature rises to 353 K, η value decreases to 60.14%. These results confirm that NCDs still possess superior inhibition effect to delay the corrosion of Q235 carbon steel even under high temperature conditions.

Table 5. Electrochemical parameters obtained from potentiodynamic polarization plots and corresponding inhibition efficiency for Q235 carbon steel in 0.1 M HCl solution in the absence and presence of 500 ppm of NCDs (1:10) under various temperatures

Samples	T (K)	i_{corr} (μA· cm^{-2})	E_{corr} (mV)	η (%)
0.1 M HCl	298	417	-519	/
	303	525	-505	/
	313	581	-500	/
	333	688	-494	/
	353	845	-495	/
500 ppm NCDs (1:10)	298	45.7	-460	89.04
	303	52.6	-458	89.98
	313	71.3	-453	87.72
	333	73.0	-450	89.39
	353	337	-445	60.14

According to the above analysis results, some useful information on the mechanism of the inhibitor action can be obtained by comparing apparent activation energy (E_a), in the absence and presence of NCDs. The E_a value can be calculated by the Arrhenius equation [8,30].

$$log(i_{corr}) = \frac{-E_a}{2.303RT} + logA \quad (6)$$

where E_a is the temperature coefficient (apparent activation energy), R is the molar gas constant, T is the thermodynamic temperature, and A is a constant.

Figure 11a presents the plots of $log(i_{corr})$ versus 1/T in the absence and presence of 500 ppm of NCDs (1:10). The E_a values calculated from the slopes of the straight lines are summarized in Table 6. The E_a value in the blank solution is 9.96 kJ·mol^{-1} while it is 32.17 kJ·mol^{-1} in the presence of 500 ppm NCDs. The higher E_a value in the presence of NCDs indicates that NCDs can act as an efficient inhibitor to suppress the charge and mass transfer reactions by forming a physical barrier, *i.e.*, adsorption film, leading to reduction in corrosion rate.

Further, the value of standard enthalpy of activation (ΔH_a^0) and standard entropy of activation (ΔS_a^0) for the dissolution of Q235 carbon steel is calculated according to the following equation [8,45,46]:

$$i_{corr} = \frac{RT}{Nh}\, exp\left\{\frac{\Delta S_a^0}{R}\right\}\, exp\left\{-\frac{\Delta H_a^0}{RT}\right\} \quad (7)$$

where h is Planck's constant and N is Avogadro's constant, R is the molar gas constant, ΔH_a^0 is the standard activation enthalpy and ΔS_a^0 is the standard activation entropy. The plots of $log(i_{corr}/T)$ versus the reciprocal of temperature in the absence and presence of 500 ppm of NCDs (1:10) are shown in Figure 11b. Straight lines are also obtained with a slope of $(-\frac{\Delta H_a^0}{2.303R})$ and an intercept of $(log\left(\frac{R}{Nh}\right) + \frac{\Delta S_a^0}{2.303R})$. ΔH_a^0 and ΔS_a^0 values are calculated and listed in Table 6. Ideally, the ΔH_a^0 value should be equal

to E_a for the same chemical reaction in electrolytic solutions. In this investigation, the ΔH_a^0 value in the absence and presence of NCDs (1:10) is 7.22 and 29.29 kJ·mol^{-1}, respectively, and there is small difference between these two values in all the cases. The positive signs of ΔH_a^0 indicate that the dissolution of steel with a endothermic process is difficult [38]. Besides, the negative value of ΔS_a^0 indicates that the activation complex in the rate determining step represents association rather than dissociation step, meaning that the disorder of the systems decreases from reactant to the activation complex [38].

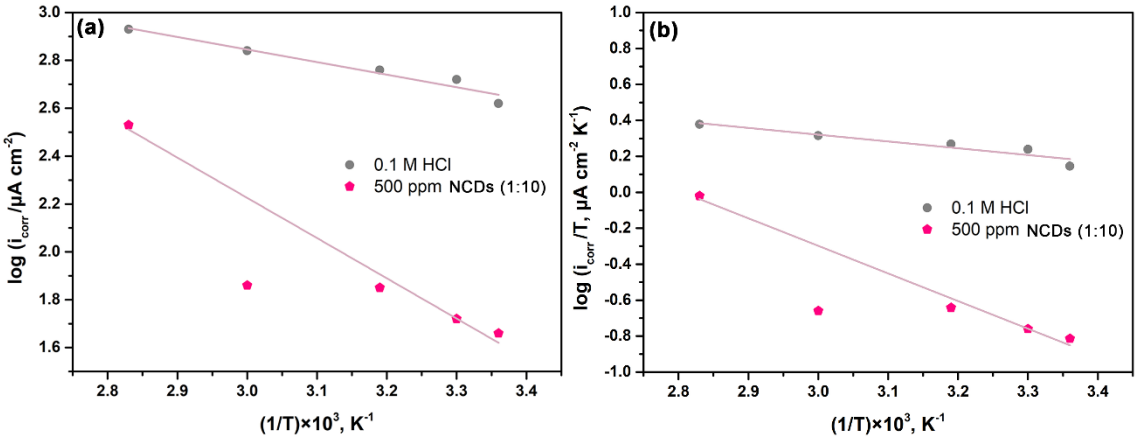

Figure 11. Arrhenius plots of and transition-state plots for Q235 carbon steel in 0.1 M HCl in the absence and presence of 500 ppm of NCDs (1:10)

Table 6. Thermodynamic activation parameters of Q235 carbon steel in 0.1 M HCl solutions with 500 ppm of NCDs (1:10) obtained from the electrochemical measurements

Thermodynamic parameters	**0.1 M HCl**	**500 ppm NCDs (1:10)**
	y=-0.52x+4.42	y=-1.68x+7.27
E_a(kJ·mol^{-1})	9.96	32.17
	y=-0.377x+1.45	y=-1.53x+4.3
ΔH_a^0 (kJ·mol^{-1})	7.22	29.29
$-\Delta S_a^0$(kJ·mol^{-1})	169.83	115.26

3.5. Possible inhibition mechanism

According to the data mentioned in the above section, it can be found that the NCDs (1:10) with high concentration of pyrrolic N can effectively inhibit the corrosion of the samples. This might be explained from two aspects. On one hand, NCDs can physically adsorb on the metal surface by electrostatic attraction between the protonated NCDs in HCl solution and negative charge on the surface. On the other hand, the pyrrolic N in NCDs can coordinate with the iron atom of Q235 carbon steel surface, therefore promoting the formation of a stable oxide layer that can improve the corrosion resistance of Q235 carbon steel in HCl solution.

4. CONCLUSIONS

In this study, NCDs with citric acid and ethanol amine as precursors have been successfully synthesized via microwave method and applied for the corrosion inhibition of Q235 carbon steel in HCl solution. The effect of molar ratio and concentration of NCDs, immersion time as well as temperature on the corrosion behavior of Q235 carbon steel in 0.1 M HCl solution was explored based on the systematic experimental and theoretical investigation. The main results can be drawn as follows:

(1) Electrochemical results indicate that nitrogen doping improves the inhibition efficiency of CDs for Q235 carbon steel in HCl solution. Especially, 500 ppm of NCDs (1:10) exhibit superior corrosion inhibition for Q235 carbon steel, which have a great relation with the concentration of pyrrolic N in NCDs. Besides, NCDs still remain good inhibition performance with prolonged immersion time, which are confirmed by weight loss measurement and surface morphological observation.

(2) The adsorption of NCDs on Q235 carbon steel obeys the Langmuir adsorption isotherm. Further, XPS analysis indicates that the pyrrolic N in NCDs and protonated NCDs in HCl solution are beneficial to the adsorption of NCDs on the Q235 carbon steel surface, leading to the superior corrosion inhibition efficiency of NCDs. Theoretical results demonstrate the stronger interactions between the free electrons of nitrogen atoms in NCDs and the unoccupied d orbital of the iron atoms.

(3) NCDs still show high corrosion inhibition efficiency (~89%) at 298~333 K although the ascending temperature can lead to the acceleration of the corrosion process of metal materials.

ACKNOWLEDGEMENTS

The authors gratefully acknowledged the financial support provided by National Natural Science Foundation of China (No. 51905278), the Special research funding from the Marine Biotechnology and Marine Engineering Discipline Group in Ningbo University, the project of Key Laboratory of Impact and Safety Engineering (Ningbo University), Ministry of Education (Project No. cj201911), the Scientific and Technological Research Program of Chongqing Municipal Education Commission, China (No. KJQN201801134) and Ningbo Science and Technology Innovation 2025 Major Project (No. 2018B10083).

CREDIT AUTHOR STATEMENT

Mingjun Cui: Conceptualization, Investigation, Data curation, Roles/Writing - original draft.
Yujie Qiang, Wei Wang and Haichao Zhao: Supervision.
Siming Ren: Formal analysis, Supervision, Writing - review & editing.

DECLARATION OF INTERESTS

The authors declare that they have no known competing financial interests or personal relationships that could have appeared to influence the work reported in this paper.

Reference

1. J. Aljourani, K. Raeissi, M.A. Golozar, *Corros. Sci.*, 51 (2009) 1836.
2. M.A. Migahed, I.F. Nassar, *Electrochim. Acta.*, 53 (2008) 2877.
3. R, Solmaz, G. Kardaş, M. Çulha, B. Yazıcı, M, Erbil, *Electrochim. Acta.*, 53 (2008) 5941.

4. Y. Qiang, S. Zhang, L. Guo, X. Zheng, B. Xiang, S. Chen, *Corros. Sci.*, 119 (2017) 68.
5. A.Khadiri, R. Saddik, K. Bekkouche, A. Aouniti, B. Hammouti, N. Benchat, M. Bouachrine, R. Solmaz, *J. Taiwan Inst. Chem.*, 58 (2016) 552.
6. G. Khan, W.J. Basirun, S.N. Kazi, P. Ahmed, L. Magaji, S.M. Ahmed, G.M. Khan, M.A. Rehman, *J. Colloid Interface Sci.*, 502 (2017) 134.
7. G. Sığırcık, T. Tüken, M. Erbil, *Appl. Surf. Sci.*, 324 (2015) 232.
8. L.L. Liao, S. Mo, H.Q. Luo, N.B. Li, *J. Colloid Interface Sci.*, 499 (2017) 110.
9. Y. Qiang, S. Zhang, B. Tan, S. Chen, *Corros. Sci.*, 133 (2018) 6.
10. P. Zuo, J. Liu, H. Guo, C. Wang, H. Liu, Z. Zhang, Q. Liu, *Anal. Bioanal. Chem.*, 411 (2019) 1647.
11. P. Zhu, D. Lyu, P.K. Shen, X. Wang, *J. Lumin.*, 207 (2019) 620.
12. S.S. Monte-Filho, S.I.E. Andrade, M.B. Lima, Araujo, *J. Pharm. Anal.*, 9 (2019) 209.
13. V. Romero, V. Vila, I. de la Calle, I. Lavilla, C. Bendicho, *Sensor. Actuat. B- Chem.*, 280 (2019) 290.
14. W. Tang, B. Wang, J. Li, Y. Li, Y. Zhang, H. Quan, Z. Huang, *J. Mater. Sci.*, 54 (2018) 1171.
15. C. Zhu, Y. Fu, C. Liu, Y. Liu, L. Hu, J. Liu, I. Bello, H. Li, *Adv. Mater.*, 29 (2017).
16. M. Cui, S. Ren, Q. Xue, H. Zhao, L. Wang, *J. Alloy. Compd.*, 726 (2017) 680.
17. M. Cui, S. Ren, H. Zhao, L. Wang, Q. Xue, *Appl. Surf. Sci.*, 443 (2018) 145.
18. Y. Ye, D. Yang, H. Chen, S. Guo, Q. Yang, L. Chen, H. Zhao, L. Wang, *J. Hazard Mater.*, 381 (2019) 121019.
19. Y. Qiang, S. Zhang, H. Zhao, B. Tan, L. Wang, *Corros. Sci.*, 161 (2019).
20. S. Ren, M. Cui, H. Zhao, L. Wang, *Surf. Topogr. Metrol.*, 6 (2018) 024003.
21. R. Solmaz, *Corros. Sci.*, 79 (2014) 169.
22. D. Daoud, T. Douadi, H. Hamani, S. Chafaa, M. Al-Noaimi, *Corros. Sci.*, 94 (2015) 21.
23. D.B. Hmamou, R. Salghi, A. Zarrouk, M.R. Aouad, O. Benali, H. Zarrok, M. Messali, B. Hammouti, Weight Loss, Electrochemical, *Ind. Eng. Chem. Res.*, 52 (2013) 14315.
24. Y. Zhang, X. Liu, Y. Fan, X. Guo, L. Zhou, Y. Lv, J. Lin, *Nanoscale*, 8 (2016) 15281.
25. W. Lu, X. Gong, M. Nan, Y. Liu, S. Shuang, C. Dong, *Anal. Chim. Acta.*, 898 (2015) 116.
26. Z. Tu, E. Hu, B. Wang, K.D. David, P. Seeger, M. Moneke, R. Stengler, K. Hu, *Friction*, (2019).
27. N. Dhenadhayalan, K.-C. Lin, R. Suresh, P. Ramamurthy, *J. Phys. Chem. C*, 120 (2016) 1252.
28. Z. Qin, W. Wang, X. Zhan, X. Du, Q. Zhang, R. Zhang, K. Li, J. Li, *Spectrochim. Acta A Mol. Biomol. Spectrosc.*, 208 (2019) 162.
29. P. Morales-Gil, M.S. Walczak, R.A. Cottis, J.M. Romero, R. Lindsay, *Corros. Sci.*, 85 (2014) 109.
30. P. Mourya, S. Banerjee, M.M. Singh, *Corros. Sci.*, 85 (2014) 352.
31. E. Kowsari, S.Y. Arman, M.H. Shahini, H. Zandi, A. Ehsani, R. Naderi, A. PourghasemiHanza, M. Mehdipour, *Corros. Sci.*, 112 (2016) 73.
32. A. Zarrouk, B. Hammouti, T. Lakhlifi, M. Traisnel, H. Vezin, F. Bentiss, *Corros. Sci.*, 90 (2015) 572.
33. A. Khadiri, A. Ousslim, K. Bekkouche, A. Aouniti, A. Elidrissi, B. Hammouti, *Portugaliae Electrochim. Acta*, 32 (2014) 35.
34. I.B. Obot, Z.M. Gasem, *Corros. Sci.*, 83 (2014) 359.
35. S. Deng, X. Li, X. Xie, *Corros. Sci.*, 80 (2014) 276.
36. M. Cui, S. Ren, J. Pu, Y. Wang, H. Zhao, L. Wang, *Corros. Sci.*, 159 (2019).
37. P.C. Okafor, Y. Zheng, *Corros. Sci.*, 51 (2009) 850.
38. M. Behpour, S.M. Ghoreishi, N. Soltani, M. Salavati-Niasari, *Corros. Sci.*, 51 (2009) 1073.
39. N.A. Odewunmi, S.A. Umoren, Z.M. Gasem, S.A. Ganiyu, Q. Muhammad, *J. Taiwan Inst. Chem.*, 51 (2015) 177.
40. D. Zhang, Y. Tang, S. Qi, D. Dong, H. Cang, G. Lu, *Corros. Sci.*, 102 (2016) 517.
41. Y. Qiang, S. Zhang, L. Wang, *Appl. Surf. Sci.*, *492* (2019) 228.
42. M. FINŠGAR, *Corros. Sci.*, 72 (2013) 90.
43. P. Mourya, P. Singh, A.K. Tewari, R.B. Rastogi, M.M. Singh, *Corros. Sci.*, 95 (2015) 71.

44. D. Briggs, M.P. Seah, *John Wiley & Sons Ltd., Sussex (Section 9.4 and Appendix 2)* (1983).
45. L.L. Liao, S. Mo, J.L. Lei, H.Q. Luo, N.B. Li, *J. Colloid. Interface Sci.*, 474 (2016) 68.
46. S.S.A.E. Rehim, H.H. Hassan, M.A. Amin, *Mater. Chem. Phys.,* 70 (2001) 64